Liquid Crystals
Publication details, including instructions for authors and subscription information:
http://www.informaworld.com/smpp/title~content=t713926090

Simulation of texture evolution for nematic liquid crystalline polymers under shear flow

Houjie Tu; Gerhard Goldbeck-Wood; Alan H. Windle

Online publication date: 11 November 2010

To cite this Article Tu, Houjie , Goldbeck-Wood, Gerhard and Windle, Alan H.(2002) 'Simulation of texture evolution for nematic liquid crystalline polymers under shear flow', Liquid Crystals, 29: 3, 335 — 345
To link to this Article: DOI: 10.1080/02678290110098656
URL: http://dx.doi.org/10.1080/02678290110098656

LIQUID CRYSTALS, 2002, VOL. 29, NO. 3, 335–345

Taylor & Francis
Taylor & Francis Group

Simulation of texture evolution for nematic liquid crystalline polymers under shear flow

HOUJIE TU, GERHARD GOLDBECK-WOOD† and ALAN H. WINDLE*
Department of Materials Science and Metallurgy, University of Cambridge, Cambridge CB2 3QZ, UK

(*Received 12 May 2001; accepted 29 June 2001*)

The development of microstructure in nematic liquid crystalline polymers under shear flow is investigated through computational simulation. By using a tensorial expression for the elastic torque, the nemato-dynamic equation is numerically resolved. The simulation shows that elastic anisotropy has a strong influence on the evolution of the director and that the 'log-rolling' orientation of the directors emerges for tumbling nematics if the twist constant is smaller than the splay and the bend constants, even though one starts from a structure in which the directors are aligned within the velocity and velocity gradient plane. The interaction of wedge disclination pairs subject to a shear flow field is also simulated. The generation, multiplication and interaction of inversion wall defects during shearing have been revealed. In general the wall moves to the boundaries and is absorbed by the boundaries. When two walls of opposite orientation meet, a loop may form, then shrink, and finally collapse. Correspondingly, if they have the same orientation, commutation will occur.

1. Introduction

Thermotropic liquid crystalline polymers (LCPs) are used for mouldings and extrusions because of their good mechanical properties, and thermal and environmental stability. One of the characteristics of LCPs is that they are rich in microstructure, and striking birefringence is observed in a mesophase of LCPs in the polarizing microscope. The orientation within an LCP can be described by a director field (**n**) [1], which is the average alignment of the molecular mesogens, and it is the discontinuities and distortions in this field which give rise to the optical textures. Another feature of LCPs is that defects can be generated and multiplied under shear flow, a phenomenon which is assumed to be associated with their rheological properties. There is considerable interest in the mechanism of the formation of these textures, their behaviour during injection or extrusion processing, and their influence on the properties of the products.

The most successful dynamical continuum theory of nematic liquid crystals (LCs) is the Ericksen–Leslie theory [1], which predicts director tumbling and flow aligning behaviour in nematic LCs under shear. It can be shown that an LC exhibits different flow-induced orientation modes, depending on various parameters [2]. If the tumbling parameter λ is equal to or greater than unity, the extensional component of the shear field dominates and the director tends toward a steady state orientation angle θ with respect to the flow direction [2]

$$\tan\theta = \left(\frac{\lambda-1}{\lambda+1}\right)^{1/2} \tag{1}$$

If $\lambda < 1$, vorticity dominates over extension and the director cannot find a steady state orientation, but tumbles continuously. The time taken for the director to rotate through an angle of 2π is found to be [2]

$$T = \frac{4\pi}{\dot{\gamma}(1-\lambda^2)^{1/2}} \tag{2}$$

where $\dot{\gamma}$ is the shear rate. Meanwhile, a 'log-rolling' phenomenon has been found in experiments [3, 4] and in numerical simulations [5–7]; here the director aligns along the vorticity axis, even though initially oriented within the shear plane, the plane containing the velocity axis and the velocity gradient axis. Figure 1 gives a schematic representation of these types of director behaviour, i.e. flow-aligning, 'log-rolling' and tumbling.

The application of the Ericksen–Leslie theory involves two coupled and time dependent fields: the velocity field $\mathbf{v}(\mathbf{r}, t)$ and the director field $\mathbf{n}(\mathbf{r}, t)$. In the literature, assumptions are usually made to simplify the velocity and the director fields or the expression of the elastic free energy. For example, the elastic terms may be

*Author for correspondence; e-mail: ahw1@cus.cam.ac.uk
†Present address: Accelrys Ltd., The Quorum, Cambridge CB5 8RE, UK.

Liquid Crystals ISSN 0267-8292 print/ISSN 1366-5855 online © 2002 Taylor & Francis Ltd
http://www.tandf.co.uk/journals
DOI: 10.1080/02678290110098656

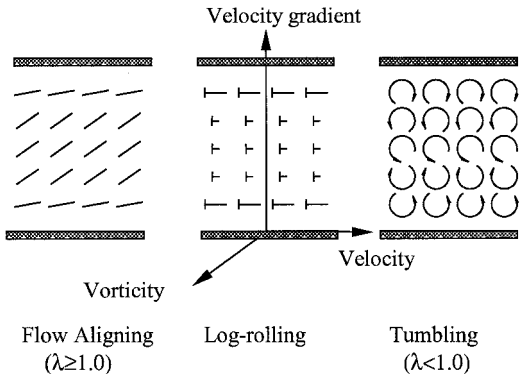

Figure 1. A schematic representation of the typical geometries for: (*a*) flow-aligning, (*b*) 'log-rolling' and (*c*) tumbling, and the definition of the coordinate system. The orientation in contact with the plates is envisaged as parallel to the velocity axis.

ignored [8] owing to the high viscosity of LCPs, while a simple shear flow, which uncouples the director and the velocity fields, has been widely used in other previous studies [5, 9–12] and enables one to focus on the effect of elasticity. Another simplifying assumption is the adoption of equal elastic constants to simplify the elastic term [10–14].

In an associated paper, a tensorial expression for the elastic torque is used as the basis for a numerical algorithm which can handle the three unequal elastic constants [15], the algorithm being calibrated through its prediction of Fréedericksz transitions. The simulation results of the evolution of defects, in the absence of an external field, show that the type of distortion dramatically depends on elastic anisotropy, see preceding paper in this issue [16]. In the present paper, the algorithm is used to simulate the dynamic behaviour of the director. The details of the governing equation are given first, and then the effect of elastic anisotropy on flow-aligning nematics and tumbling nematics is described. Finally, the evolution of the wedge disclination under a shear flow is investigated.

2. Dynamic model

The Ericksen–Leslie equation that describes the evolution of the director is [1]

$$\frac{\partial \mathbf{n}}{\partial t} + \mathbf{v} \cdot \nabla \mathbf{n} = \mathbf{\Omega} \cdot \mathbf{n} + \lambda(\mathbf{\Gamma} \cdot \mathbf{n} - \mathbf{\Gamma} : \mathbf{nnn}) + \frac{1}{\gamma_1}(\mathbf{h} - \mathbf{h} \cdot \mathbf{nn}) \tag{3}$$

where $\mathbf{\Gamma}$ and $\mathbf{\Omega}$ are the symmetric and antisymmetric parts of the velocity ($\mathbf{v}$) gradient tensor, which represent the extensional and rotational effects, respectively, γ_1 and λ are the rotational viscosity coefficient and the tumbling parameter, respectively and $\mathbf{h}$ is the 'texture field' generated by the spatial inhomogeneity of the director. A tensorial form of the Frank free energy leads to the following expression for $\mathbf{h}$ [15]

$$h_\beta = 2n_\alpha \Big\{ k_2 \Delta n_\alpha n_\beta + (k_1 - k_2)[\nabla_{\alpha\gamma} n_\gamma n_\beta + \nabla_{\beta\gamma} n_\gamma n_\alpha] + (k_3 - k_1)\left[\nabla_\gamma (n_\gamma n_\lambda \nabla_\lambda n_\alpha n_\beta) - \frac{1}{2} \nabla_\alpha n_\gamma n_\lambda \nabla_\beta n_\gamma n_\lambda \right] \Big\} \tag{4}$$

where the Greek subscripts refer to the Cartesian components. The summation convention is used here, and

$$\nabla_\alpha = \frac{\partial}{\partial x_\alpha}, \quad \nabla_{\alpha\beta} = \frac{\partial^2}{\partial x_\alpha \partial x_\beta}, \quad \mathbf{r} = (x_1, x_2, x_3) = (x, y, z)$$

and k_1, k_2 and k_3 are the Frank elastic constants which are associated with splay, twist and bend deformations, respectively.

A simple shear flow is used throughout this paper. The coordinate system and the shear flow geometry are shown in figure 2. The origin of the coordinate system is in the centre of the sample. For simple shear flow, if the shear rate is $\dot{\gamma}$, then

$$\mathbf{v} = \begin{pmatrix} \dot{\gamma} x_2 \\ 0 \\ 0 \end{pmatrix} \quad \mathbf{\Gamma} = \frac{1}{2}\begin{pmatrix} 0 & \dot{\gamma} & 0 \\ \dot{\gamma} & 0 & 0 \\ 0 & 0 & 0 \end{pmatrix} \quad \mathbf{\Omega} = \frac{1}{2}\begin{pmatrix} 0 & \dot{\gamma} & 0 \\ -\dot{\gamma} & 0 & 0 \\ 0 & 0 & 0 \end{pmatrix} \tag{5}$$

To render equation (3) dimensionless, we set

$$t^* = t\dot{\gamma}, \quad x_\alpha^* = \frac{x_\alpha}{D} \tag{6}$$

where D is the distance between the two plates. Omitting '*' in the final forms for the sake of simplicity,

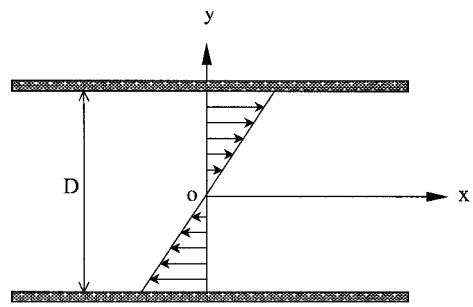

Figure 2. A schematic representation of simple shear flow. The *x*, *y* and *z* are the flow direction, the velocity gradient direction and the vorticity direction respectively. The vorticity direction (*z*) is perpendicular to the paper *or* the shear plane (*xOy*).

equation (3) becomes

$$\frac{\partial n_1}{\partial t} = \frac{1}{2} n_2 [\lambda(1 - 2n_1 n_1) + 1] - x_2 n_\alpha \nabla_1 n_1 n_\alpha + \frac{1}{E_r} g_1 \tag{7}$$

$$\frac{\partial n_2}{\partial t} = -\frac{1}{2} n_1 [\lambda(2n_2 n_2 - 1) + 1] - x_2 n_\alpha \nabla_1 n_2 n_\alpha + \frac{1}{E_r} g_2 \tag{8}$$

$$\frac{\partial n_3}{\partial t} = -\lambda n_1 n_2 n_3 - x_2 n_\alpha \nabla_1 n_3 n_\alpha + \frac{1}{E_r} g_3 \tag{9}$$

where

$$E_r = \frac{\gamma_1 V D}{k} \tag{10}$$

is the Ericksen number,

$$k = \max(k_1, k_2, k_3) \tag{11}$$

is the largest elastic constant, $V = \dot{\gamma} D$ is the characteristic velocity and the $g_i (i = 1, 2, 3)$ correspond to the final term of the right hand side of equation (3), and are made dimensionless. In general

$$g_i = g_i(n_\alpha n_\beta, \nabla_\alpha n_\beta n_\gamma, \nabla_{\alpha\beta} n_\gamma n_\theta, k_\alpha / k). \tag{12}$$

The director field in our approach is represented by a set of directors in the cells of a spatially fixed cubic lattice. For a given initial pattern and boundary conditions, equations (7–9) can be integrated numerically

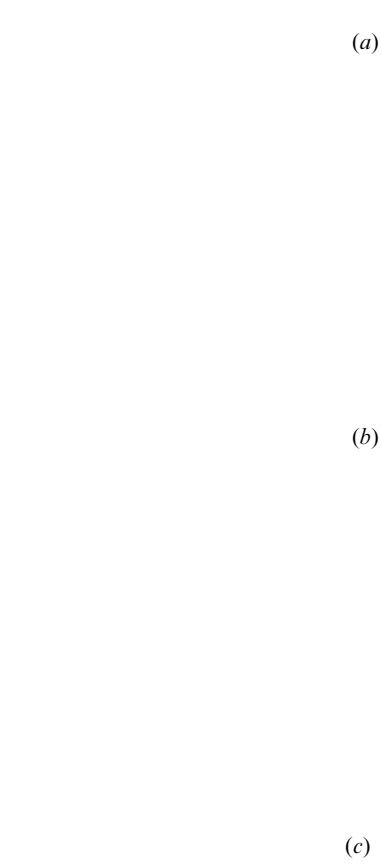

Figure 3. Flow-aligning angles of different layers in the y direction with $\lambda = 2.0$ at different Ericksen numbers: (*a*) 4.0, (*b*) 40.0 and (*c*) 400.0. Cases 0, 1, 2, 3 and 4 refer to $k_1 = k_2 = k_3 = 0$, $k_1 = k_2 = k_3$, $10k_1 = k_2 = k_3$, $k_1 = 10k_2 = k_3$, $k_1 = k_2 = 10k_3$ respectively.

Figure 4. Free energy plots of the tumbling nematics with $\lambda = 0.5$ at different Ericksen number: (*a*) 40.0 and (*b*) 400.0/s. Cases 1, 2, 3 and 4 have the same meaning as in figure 3. The free energies are normalized by the maximum value seen under any conditions (i.e. the peak values for case 1).

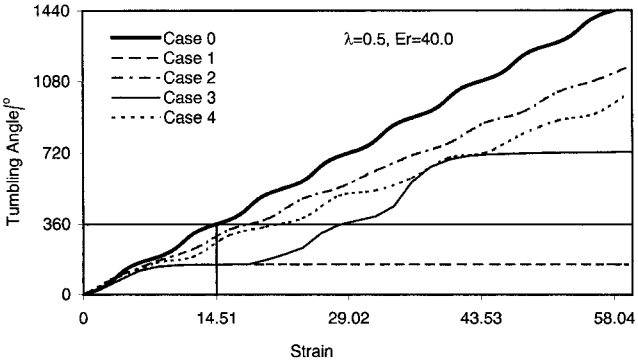

Figure 5. Tumbling angle of the director in the centre of a cell with $\lambda = 0.5$ and the Ericksen number 40.0. Cases 1, 2, 3 and 4 have the same meaning as in figure 3, and case 0 represents no elasticity.

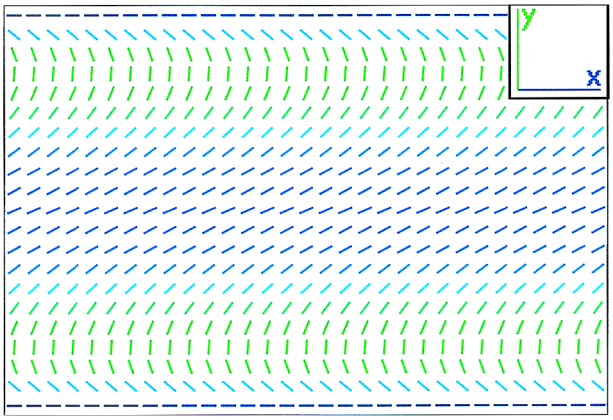

Figure 6. An xOy slice of the director pattern with $\lambda = 0.5$ and $k_1 = k_2 = k_3$; every plane has the same configuration. The colour coding in this and further similar figures is an additional indication of orientation with variation across the blue–green part of the spectrum corresponding to the director orientation between the x and y axes.

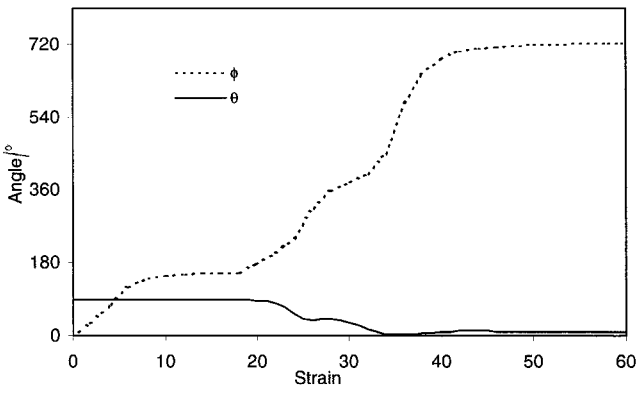

Figure 7. Spherical angles ϕ and θ of the director in the centre of the cell with $\lambda = 0.5$ and the Ericksen number 40.0 in case 3.

by a standard technique in which the finite difference scheme is used to discretize the elastic and the convective terms.

3. Shearing of defect-free structures

As mentioned above, flow-aligning and tumbling are analytically predicted for nematics if no elastic effect is considered. However, it is beyond doubt that elastic anisotropy has a strong effect on the microstructures of nematic LCPs, and the current algorithm is used to simulate how elastic anisotropy affects the behaviour of the directors under a simple shear flow.

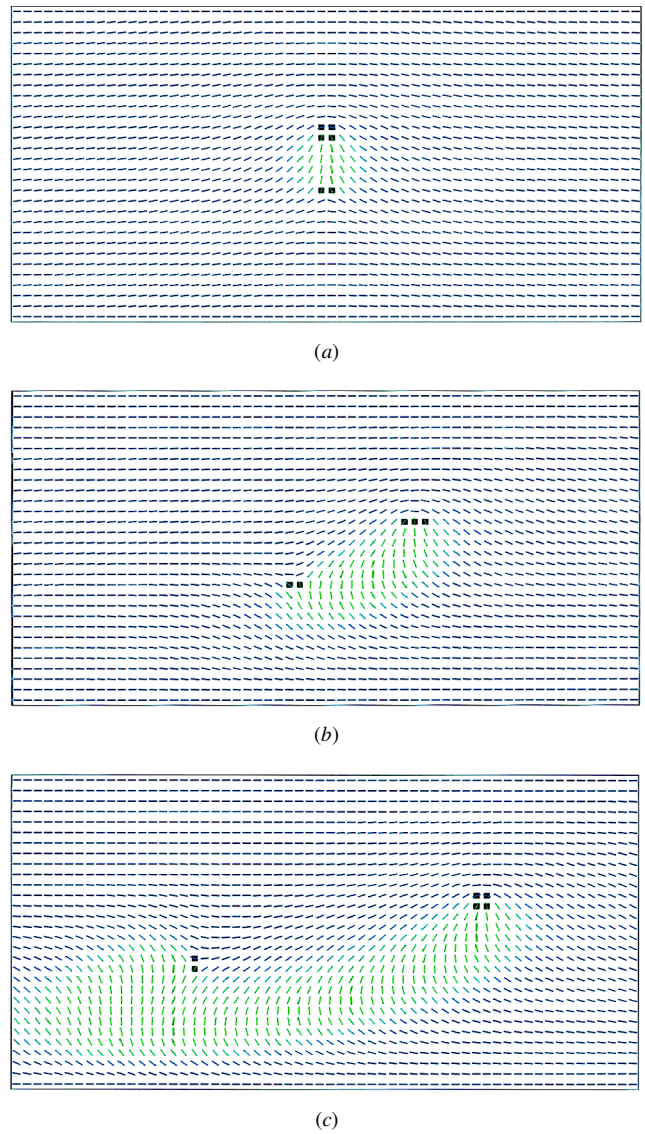

(*a*)

(*b*)

(*c*)

Figure 8. Evolution of the half-disclination pair under shear flow. The director patterns at different time steps are given: (*a*) time step 0, (*b*) time step 2000 and (*c*) time step 4000.

In this section, the following cases (0, 1, 2, 3 and 4), refer to the situations where $k_1 = k_2 = k_3 = 0$, $k_1 = k_2 = k_3$, $10k_1 = k_2 = k_3$, $k_1 = 10k_2 = k_3$ and $k_1 = k_2 = 10k_3$, respectively. These have been chosen to represent the cases of no elasticity, equal constants, small splay constant, small twist constant and small bend constant, respectively. The simulations are performed on a $31 \times 21 \times 11$ lattice, using planar boundary conditions in the velocity gradient direction and periodic boundary conditions in the directions of both velocity and vorticity. The initial pattern is a mono-domain, oriented in the velocity direction.

3.1. *Flow-aligning and the boundary effect*

According to theory [2], for flow-aligning nematics ($\lambda \geqslant 1.0$), the viscous torque will drive the director to tilt towards the flow direction with a given angle. The elastic torque is expected to affect the distribution of the directors via the imposed boundary conditions. The equilibrium state is the one in which these two kinds of torques are balanced. The current model can be used to reveal the existence of the boundary layer.

Figure 3 shows the flow-aligning angles of the directors in different layers with the y direction, using $\lambda = 2.0$, for different Ericksen numbers and elastic constants. According to equation (1), the flow-aligning angle should be 30° in this case without elasticity. As shown in figure 3, the elastic constants have an effect on the flow-aligning angles. If no elastic effect is considered (case 0), the flow-aligning angle is consistent with the theoretical result. In all other cases, the pattern is affected by the boundaries. If the Ericksen number is very small, for example $E_r = 4.0$,

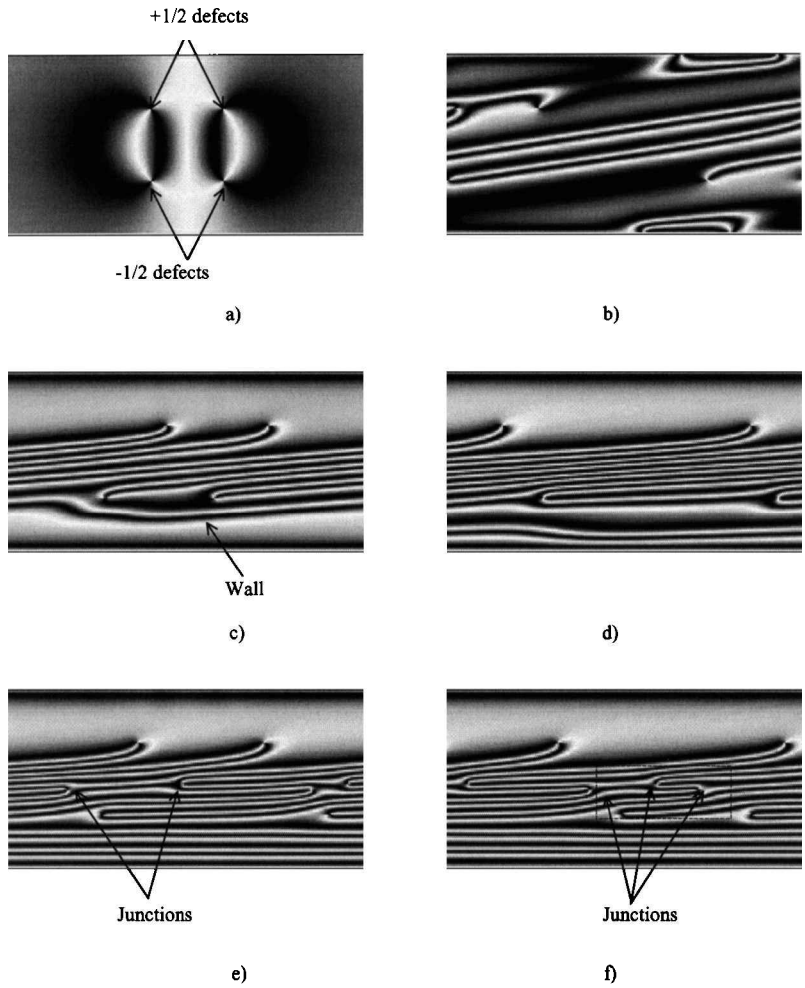

Figure 9. Polarized light intensity profiles at different time steps with $\lambda = 1.0$, $E_r = 1000.0$, $k_1 = k_2 = k_3 = 10^{-11}$ N, $\Delta t = 10^{-3}$ s. Homeotropic and periodic boundary conditions are used for the y and the x directions, respectively. The lattice used is $200 \times 100 \times 1$. The initial pattern has two 'parallel' defect pairs. Time step: (*a*) 0, (*b*) 7000, (*c*) 13 000, (*d*) 18 000, (*e*) 36 000 and (*f*) 43 000. The corresponding director distribution within the dashed square area of (*f*) is given in figure 11 (*a*).

the elastic effect dominates the pattern; see figure 3 (*a*). If the Ericksen number is increased to $E_r = 40.0$ and $E_r = 400.0$—figures 3 (*b*) and 3 (*c*), respectively—a flow-aligning domain is established in the centre, with the same flow-aligning angle as predicted by equation (1). Meanwhile, the boundary layer becomes narrower.

In this specific configuration, the flow-aligning angles are not sensitive to the twist and bend constants. As shown in figure 3, cases 1, 3 and 4 have similar distribution of flow-aligning angles. However the boundary layers of case 2 are thinner than any of the other cases. The reason for this is that the distortion in boundary layers has no twist component and is predominantly of the splay type; therefore the elastic torque mainly decreases with the splay constant in this particular configuration.

3.2. *Tumbling and 'log-rolling'*

Theoretical analysis has revealed that, for tumbling nematics ($\lambda < 1.0$), the director will continuously rotate in the shear plane [2]. However, in some circumstances, elastic torque will result in 'log-rolling' of the directors where the elastic torque drives the directors out of the shear plane and they eventually orient along the vorticity direction.

If the initial structure is an in-plane structure, for example, a mono-domain configuration, the directors will rotate within the shear plane as shown by the plots of the total free energy of the system in figure 4. Figure 4 (*a*) shows that tumbling occurs in cases 2 and 4, in which the system has either a lower splay or a lower bend constant, with $E_r = 40.0$. However, the director does not keep rotating in the case of equal constants

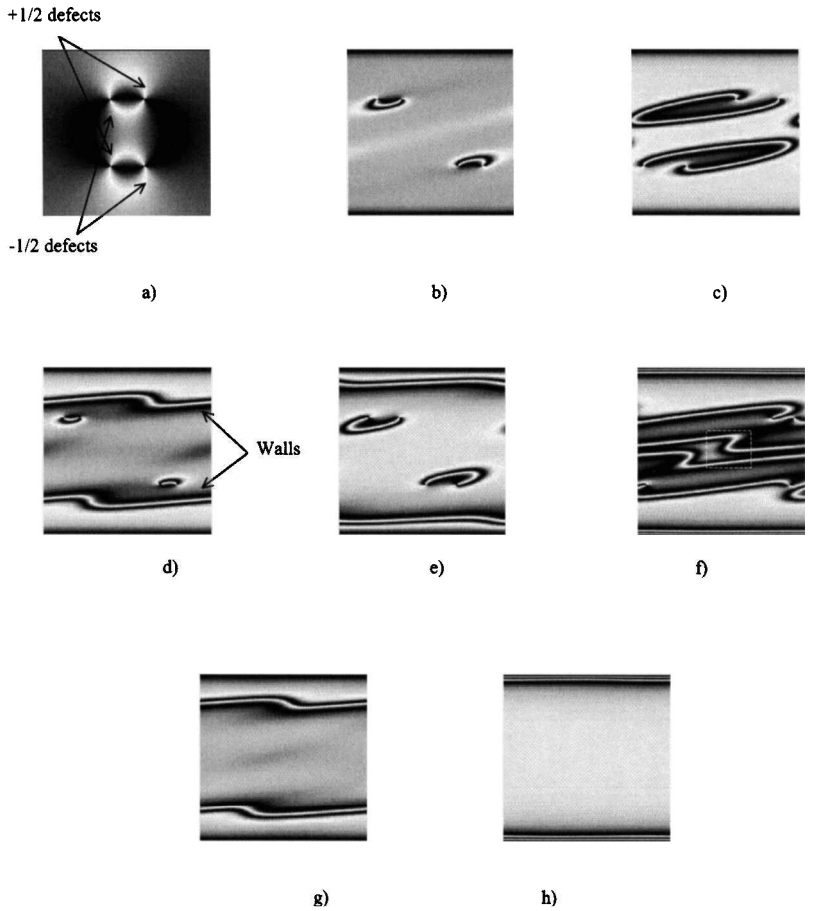

Figure 10. Polarized light intensity profiles at different time steps with $\lambda = 1.0$, $E_r = 1000.0$, $k_1 = k_2 = k_3 = 10^{-11}$ N, $\Delta t = 10^{-3}$ s. Homeotropic and periodic boundary conditions are used for the y and the x directions, respectively. The lattice used is $200 \times 200 \times 1$. The initial pattern has two 'antiparallel' defect pairs. Time step: (*a*) 0, (*b*) 4000, (*c*) 12 000, (*d*) 19 000, (*e*) 25 000, (*f*) 33 000, (*g*) 38 000 and (*h*) 50 000. Two walls are generated in (*d*) and the walls move toward the boundaries as shown in (*e*); they are absorbed by the boundaries, see (*f*). The corresponding director distribution within the dashed square area in (*f*) is given in figure 11 (*b*); (*h*) shows flow-aligning and a defect free pattern.

(case 1). This shows that the system can find a balance between the elastic torque and the viscous torque. The balance is broken if the Ericksen number is increased, as shown in figure 4(*b*), in which the Ericksen number is 400.0. If the twist constant is smaller than the splay and the bend constants (case 3), the directors cannot maintain tumbling within the shear plane, as shown in both figures 4(*a*) and 4(*b*). Instead, the directors eventually turn into the vorticity direction, which is the energetically favoured state.

According to equation (4), when starting from the in-plane structure, i.e. $n_3 = 0$, we have $h_3 = 0$ and it leads to there being no out-of-plane component according to equation (9). The only reason for the 'log-rolling' of the directors is that a small disturbance is amplified and the bifurcation of the stable state develops if the twist constant is small enough. In the simulations, the disturbance is the numerical truncation error. In the physical world, a fluctuation could be considered as the disturbance. The interesting point is that we can only see this bifurcation in the case of a low twist constant. In the other cases, the numerical truncation error seems not to be amplified. This coincides with the observation of 'log-rolling' in some LCPs during shearing [3, 4], as the twist constant is proposed to be the lowest for main chain LCPs.

The variation of the rotation angle (ϕ) of the director with the strain, in the cell at the centre of the bulk, is presented in figure 5. According to equation (2), the strain period is $\dot{\gamma}T = 14.51$ for $\lambda = 0.5$ during which the director rotates through an angle of 2π without the elastic effect. The computational result is in good agreement with the theoretical prediction in the case of no elasticity (case 0). It takes longer time for the director to rotate by an angle of 2π, when the splay or the bend constant is smaller than the others, as in cases 2 and 4 shown in figure 5. With the condition of equal elastic constants (case 1 in figure 5), the director shows a flow-aligning characteristic. It rotates at the beginning and then finds a stable state. The stable director field is shown in figure 6.

With a small twist constant (case 3 in figure 5), the evolution of the director is the same as in the case of equal elastic constants until the bifurcation develops. As a result, the director loses its stable orientation and points out-of-plane. It gradually turns to the vorticity direction. Simultaneously, the director keeps rotating about the vorticity axis. In other words, the director performs a motion which has been described as 'kayaking' until it reaches another stable state. Figure 7 gives the variation of ϕ (the angle between the director and the velocity direction in the shear plane) and θ (the angle between the director and the vorticity axis) with strain. It clearly shows two plateaus, corresponding to the two steady states. The second plateau shown in figure 7 refers to the log-rolling state.

4. Shearing of wedge disclination pairs: a two dimensional simulation

LCPs are found to show rich textures under shear flow, but how these textures are created is still unclear. The high viscosity of LCPs makes it difficult to remove all the defects in the samples, especially in the case of thermotropic LCPs. The defects observed, both in experiments and numerical simulations, are often half strength disclinations and they always appear in pairs. So it is worthwhile to simulate the behaviour of pairs of half-disclination under a shear flow.

For the sake of simplicity, a two-dimensional model is used. This 2D simulation can also be compared with an experimental observation of a very thin nematic sample under a steady shear condition using a parallel plate rheometer or optical shear cell. Whereas the simulations may provide the information of texture evolution

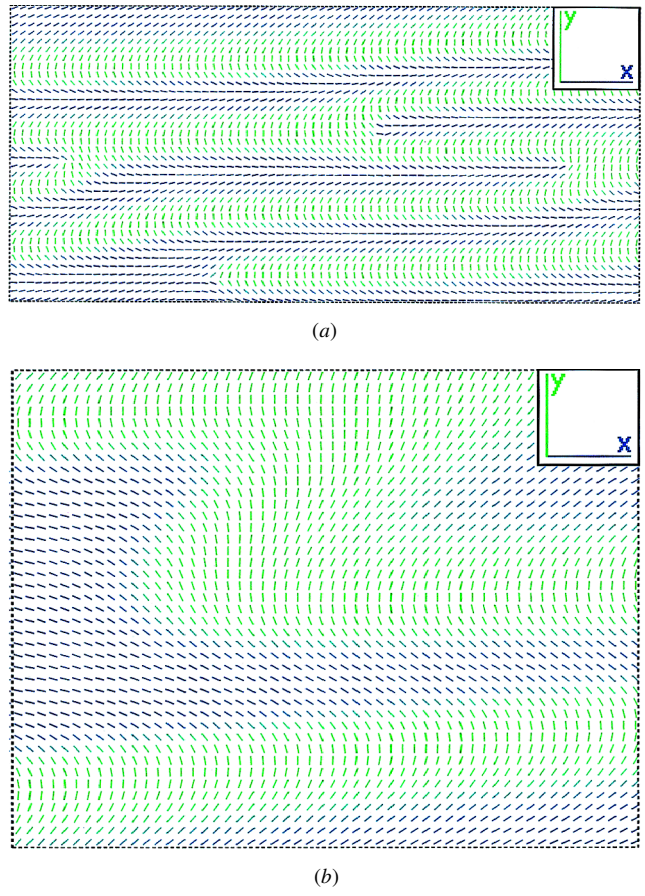

(*a*)

(*b*)

Figure 11. Typical director distribution of the inversion walls: (*a*) 'parallel' walls, corresponding to figure 9(*f*); (*b*) 'antiparallel' walls, corresponding to figure 10(*f*).

in the shear plane, it is not easy to observe this experimentally. Using a rheo-optical technique, the texture evolution can be viewed in the plane perpendicular to the direction of the velocity gradient. The results of these observations should be viewed as an average of all of the layers. Numerical simulation can therefore be helpful in understanding this issue. In the simulations reported below, we have set the model parameters to the following values: $\lambda = 1.0$ for flow aligning, $k_1 = k_2 = k_3 = 1.0 \times 10^{-11}$ N. Homeotropic and periodic boundary conditions are used for the y and x directions, respectively.

4.1. *Deformation of a wedge disclination pair under shear flow*

We start from a single wedge disclination pair. The behaviour of the pair of half-disclinations is essential to our understanding of the interaction of the wedge disclination pairs under shear flow. The initial pattern can be generated by the following equations [17]

$$n_1 = \cos\phi, \quad n_2 = \sin\phi \tag{13}$$

$$\phi = \phi_0 + 0.5 \arctan \frac{y - y_1}{x - x_1} - 0.5 \arctan \frac{y - y_2}{x - x_2} \tag{14}$$

where (x_1, y_1) and (x_2, y_2) are the coordinates of the $+1/2$ and $-1/2$ defect cores, respectively, and ϕ_0 is a constant that defines the relative orientation between the two defects.

Figure 8 shows the patterns of the director at different time steps. The lattice is 60×30 with planar boundary conditions in the y direction and free boundary conditions in the x direction, and $k_1 = k_2 = k_3$ is used. Due to the convectional effect, $+1/2$ and $-1/2$ disclination move upstream and downstream, respectively. The distortion between the $+1/2$ disclination and the $-1/2$

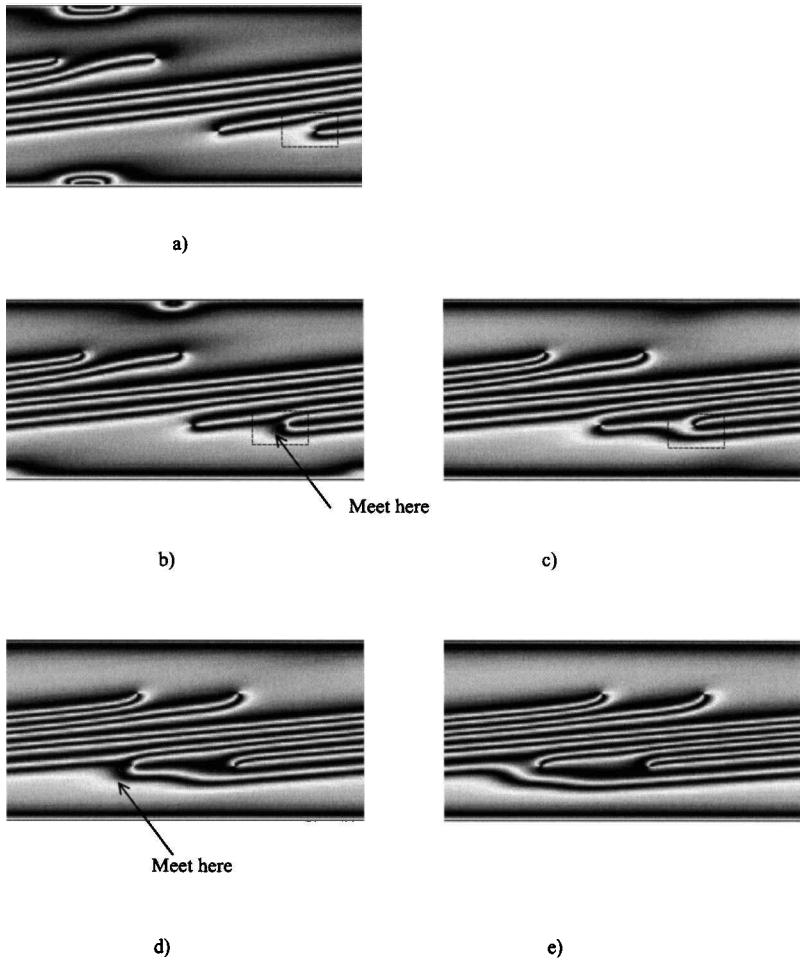

Figure 12. Interaction of the two 'parallel' walls. The conditions of the simulation are the same as that in figure 9. At time step: (*a*) 9000, (*b*) 10 000, (*c*) 11 000, (*d*) 12 000 and (*e*) 13 000.

disclination is stretched to form a wall structure. It shows that the $+1/2$ disclination conserves its own orientation with respect to the wall as the strain is increased, while the orientation of the $-1/2$ disclination rotates clockwise. This causes the wall in the vicinity of the $-1/2$ disclination to rotate and wind up. Lavine and Windle [13] gave a detailed explanation of this phenomenon, and considered three-dimensional implications.

4.2. *Interaction of wedge disclination pairs under shear flow*

The key point of the behaviour of a single half-disclination pair under shear flow is the formation of an inversion wall. In reality, there is always a host of defects in the system, and as a next stage we consider the interaction between two pairs of half-disclinations.

The superposition rule is valid in the case of equal elastic constants, so the initial pattern can be described by the following equation

$$\phi = \phi_0 + 0.5\left(\arctan\frac{y-y_1}{x-x_1} + \arctan\frac{y-y_3}{x-x_3}\right) - 0.5\left(\arctan\frac{y-y_2}{x-x_2} + \arctan\frac{y-y_4}{x-x_4}\right) \quad (15)$$

where (x_1, y_1) and (x_3, y_3) are the coordinates of the cores of the two $+1/2$ disclinations, (x_2, y_2) and (x_4, y_4) are the coordinates of the cores of the two $-1/2$ disclinations.

In the following simulations, two kinds of initial patterns are used. These are 'parallel' defect pairs and 'antiparallel' defect pairs, in which the lines starting from the core of the $-1/2$ defect to the core of the $+1/2$ defect are parallel and antiparallel, respectively. Homeotropic boundary conditions are used in the y direction and periodic boundary conditions are used in the x direction.

Figures 9 and 10 give predicted polarized light intensity profiles at different time steps during shearing. The lattice size in figure 9 is $200 \times 100 \times 1$ and $E_r = 1000$. The initial director distribution, with two 'parallel' defect pairs, is shown in figure 9 (*a*), where $\phi_0 = 0$. Figure 9 shows that the textures are generated and deformed under shearing. Figure 10 is an example starting from two 'antiparallel' defect pairs. The lattice used is $200 \times 200 \times 1$, $E_r = 2000$, and $\phi_0 = 0.375\ \pi$.

Wall defects can be observed from both simulations (figures 9 and 10) as a result of shearing. The observed evolution of the textures stems from a combination of the viscous torque and the interaction of the two pairs of disclinations. A close examination of these two simulations reveals that different initial patterns can give rise to very different texture evolution. In both cases the walls tend to align along the flow direction due to the velocity gradient. They are also found to move towards the boundaries and to be eventually absorbed by the boundaries. For example, in figure 10 two walls gradually either move up or move down to the boundaries, from time cycle 19 000 to time cycle 25 000 as shown in figures 10 (*d*) and 10 (*e*). These two walls disappear as shown in figure 10 (*f*). In figure 10 (*h*), i.e. in the 'antiparallel' case, all defects are finally annihilated and the system reaches flow-aligning with two very thin boundary layers.

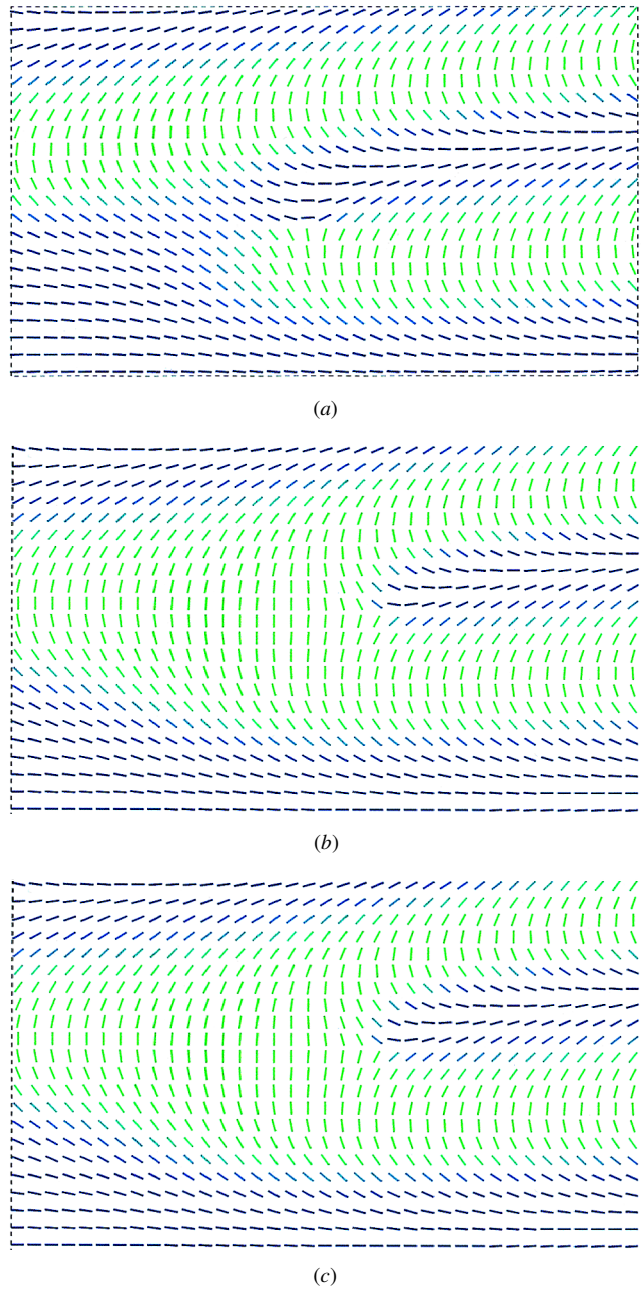

Figure 13. Director maps (*a–c*) in the local area highlighted by the dashed rectangle in figures 12 (*a–c*), respectively.

However, if the initial pattern has two 'parallel' defect pairs as in figure 9, a large number of walls can be generated and maintained before disappearing at the boundaries. 'Junctions' can be formed by the interaction between the walls, as shown in figures 9 (*e*) and 9 (*f*). The 'junctions' can be seen from the director distribution, highlighted in figure 9 (*f*) and shown in detail in figure 11 (*a*). The director is generally parallel to the flow-aligning direction except in the region of the wall. The change in the director orientation is 180° on crossing the wall.

Corresponding to the 'parallel' and 'antiparallel' pairs, two types of walls are observed: 'parallel' and 'antiparallel' walls. Figure 11 (*a*) gives the director field of 'parallel' walls and shows that the distortions in all the walls have the same orientation. Figure 11 (*b*) gives the director field of 'antiparallel' walls, which is highlighted (dashed square) in figure 10 (*f*), and shows that the distortions in all the walls have the opposite orientation.

When two walls meet, the interaction between them mainly depends on the type of these walls, i.e. 'parallel' or 'antiparallel'. If two 'parallel' walls meet, they will interpenetrate each other. Figure 12 gives an example. Two walls near the bottom plate meet as shown in figures 12 (*b*) and 12 (*d*). The results of the interaction of these two walls can be described as follows and are shown in figures 12 (*c*) and 12 (*e*), respectively. One end of the first wall attaches to the middle of the second wall. The second wall has now been divided into two parts, one of which combines with the first wall and forms a new wall. The other part is separate from the new wall. The director maps of the local areas are given

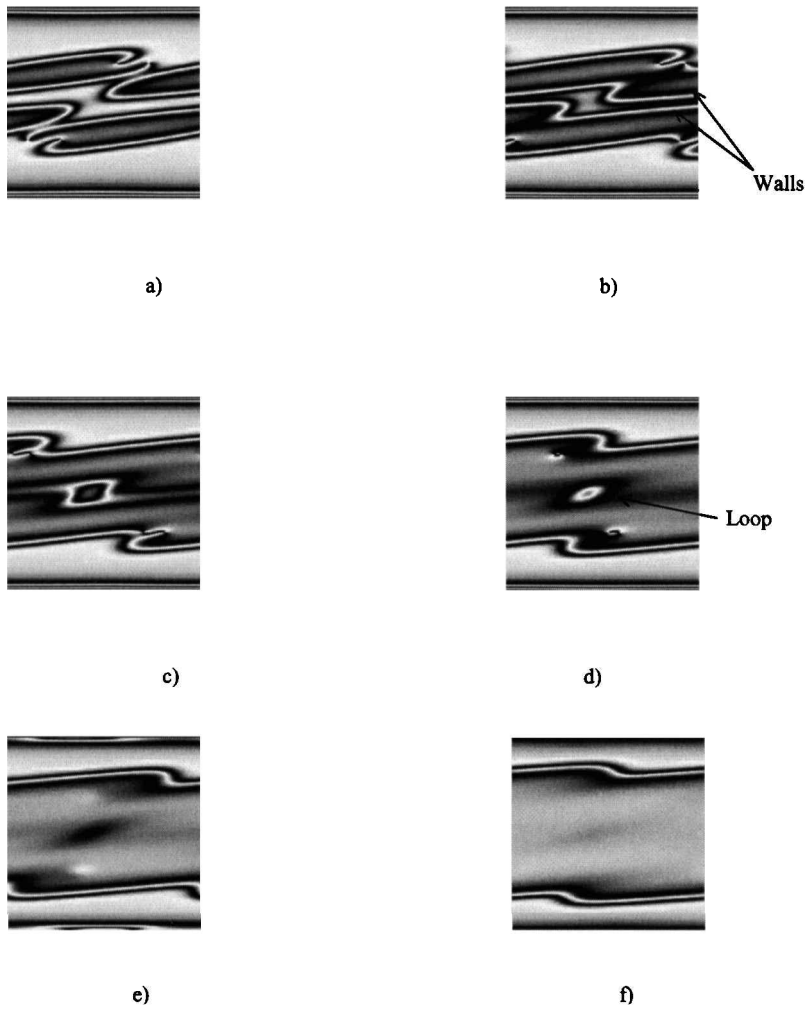

Figure 14. Interaction of two 'antiparallel' walls. The conditions of the simulation are the same as for figure 10. At time step: (*a*) 32 000, (*b*) 33 000 and two walls emerge, (*c*) 34 000 and the two walls meet, (*d*) 35 000 and a loop generates, (*e*) 36 000 and the loop is shrinking, (*f*) 38 000 and finally the loop disappears.

in figure 13. When two antiparallel walls meet, two walls unite to generate a loop, as shown in figure 14. The loop keeps shrinking and finally collapses. Therefore, a flow-aligning can be achieved in this case. Defect pairs are randomly oriented in a real system, so both the textures simulated in figures 13 and 14 are expected to emerge simultaneously.

5. Concluding remarks

The nemato-dynamics equation has been used to simulate the behaviour of nematic LCPs under shear flow. The elastic effect of textures is taken into account by using a tensorial expression of the elastic torque.

The effect of elastic anisotropy on the behaviour of the directors under shear flow has been numerically simulated. If no elastic torque is considered, the numerical results are the same as the analytic results. 'Log-rolling' orientation of the directors emerges for the tumbling nematics if the twist constant is smaller than the others, even though one starts from an in-plane structure. It suggests that tumbling nematic LCPs tend to 'log-rolling' under shear flow since a typical thermotropic LCP has a high splay constant and a low twist constant.

The interaction of wedge disclination pairs under shear flow has been investigated. Starting from different spatial configurations, wall generation, multiplication, interaction and annihilation are all observed. The initial defects and their relative orientation determine the texture evolution during shearing. A large number of parallel walls can be generated from two 'parallel' defect pairs. The 'parallel' walls can maintain and interpenetrate each other. 'Antiparallel' walls are formed from two 'anti-parallel' defect pairs; they may connect together to form a loop and eventually collapse. Thus for a flow-aligning situation, the presence of disclinations can generate wall-type defects which will increase in density with increasing strain.

The authors would like to thank the EPSRC for support under its 'Processing of conventional structural materials' programme.

References

[1] De Gennes, P. G., and Prost, J., 1993, *The Physics of Liquid Crystals* (Oxford: Clarendon Press).
[2] Larson, R. G., 1990, *Macromolecules*, **3,** 3983.
[3] Romo-Uribe, A., and Windle, A. H., 1996, *Macromolecules*, **29,** 6246.
[4] Burghardt, W. R., 1998, *Macromol. Chem. Phys.*, **199,** 471.
[5] Goldbeck-Wood, G., Coulter, P., Hobdell, J. R., Lavine, M. S., Yonetake, K., and Windle, A. H., 1998, *Mol. Simul.*, **21,** 143.
[6] Han, W. H., and Rey, A. D., 1993, *J. Non-Newtonian Fluid Mech.*, **48,** 181.
[7] Rey, A. D., 1990, *J. Rheol.*, **34,** 425.
[8] Chang, R., Shiao, F., and Yang, W., 1994, *J. non-Newtonian fluid Mech.*, **55,** 1.
[9] Rey, A. D., and Tsuji, T., 1998, *Macromol. Theory Simul.*, **7,** 623.
[10] Denniston, C., 1996, *Phys. Rev. B*, **54,** 6272.
[11] Derfel, G., 1998, *Liq. Cryst.*, **24,** 829.
[12] Derfel, G., and Radomska, B., 1997, *Liq. Cryst.*, **23,** 741.
[13] Lavine, M. S., and Windle, A. H., 1997, *Macromol. Symp.*, **124,** 35.
[14] Goldbeck-Wood, G., and Windle, A. H., 1999, *Rheol. Acta*, **38,** 537.
[15] Tu, H., Goldbeck-Wood, G., and Windle, A. H., 2001, *Phys. Rev. E*, **64,** 011704.
[16] Tu, H., Goldbeck-Wood, G., and Windle, A. H., 2002, *Liq. Cryst.*, **29,** 325.
[17] Nehring, J., and Saupe, A., 1972, *J. Chem. Soc. Faraday Trans. II*, **68,** 1.